Geophysical Research Letters

RESEARCH LETTER
10.1029/2024GL113531

Mechanisms Linking Stratospheric Gravity Wave Activity to Hurricane Intensification: Insights From Model Simulation of Hurricane Joaquin

X. Wu[1,2], L. Hoffmann[3], C. J. Wright[4], N. P. Hindley[4], M. J. Alexander[5], X. Wang[1,6], B. Chen[7], Y. Wang[1,2], and M. Li[1,2]

[1]Laboratory of Middle Atmosphere and Global Environment Observation, Institute of Atmospheric Physics, Chinese Academy of Sciences, Beijing, China, [2]University of Chinese Academy of Sciences, Beijing, China, [3]Jülich Supercomputing Centre, Forschungszentrum Jülich, Jülich, Germany, [4]Centre for Climate Adaptation and Environment Research, University of Bath, Bath, UK, [5]NorthWest Research Associates, CoRA Office, Boulder, CO, USA, [6]State Key Laboratory of Atmospheric Environment and Extreme Meteorology, Institute of Atmospheric Physics, Chinese Academy of Sciences, Beijing, China, [7]Key Laboratory of Atmospheric Environment and Processes in the Boundary Layer Over the Low-Latitude Plateau Region, Department of Atmospheric Science, Yunnan University, Kunming, China

Abstract Previous studies based on satellite observations and model simulations have revealed a significant correlation between intense stratospheric gravity wave (GW) activity and hurricane intensification. This research further investigated the underlying mechanism of this correlation by analyzing the properties and propagation characteristics of stratospheric GWs excited by Hurricane Joaquin based on a Weather Research and Forecasting model simulation. By employing the 3-D Stockwell wave analysis method, we found that GWs excited during hurricane intensification display relatively higher intrinsic frequencies, shorter horizontal wavelengths, and longer vertical wavelengths than during weakening. Analysis of these GWs' propagation using the GROGRAT ray-tracing model revealed that they can reach the middle stratosphere rapidly within 20 min. This quick propagation enabled the observation of intense stratospheric GWs before the hurricane reached its peak intensity, offering a potential indicator for hurricane intensification. These findings strengthened the basis for considering stratospheric GW activity as a proxy for hurricane intensification under specific conditions.

Plain Language Summary Hurricanes are known for their devastating impact, and recent studies indicate a strong link between stratospheric gravity waves (GWs) and the intensification of hurricanes. Our research focused on understanding this link. We found that during hurricane intensification, GWs exhibited unique characteristics. Remarkably, these waves could quickly reach the middle stratosphere in about 20 min. This rapid movement may increase the possibility of detecting these GWs before the hurricane achieves its peak intensity. The presence of these intense stratospheric GWs might act as an early warning signal, indicating that the hurricane is intensifying. This finding offers new possibilities for monitoring hurricane intensification by detecting intense stratospheric GW activity.

Key Points:

- This study provides further evidence for using stratospheric gravity wave (GW) activity as a proxy for hurricane intensification
- GWs excited during hurricane intensification display higher frequencies, longer vertical wavelengths, and shorter horizontal wavelengths
- GWs excited during hurricane intensification have a greater possibility of reaching the stratosphere before the hurricane reaches peak intensity

Supporting Information:

Supporting Information may be found in the online version of this article.

Correspondence to:

L. Hoffmann, X. Wang and B. Chen,
l.hoffmann@fz-juelich.de;
wangx2003@mail.iap.ac.cn;
chenbing@ynu.edu.cn;

Citation:

Wu, X., Hoffmann, L., Wright, C. J., Hindley, N. P., Alexander, M. J., Wang, X., et al. (2025). Mechanisms linking stratospheric gravity wave activity to hurricane intensification: Insights from model simulation of Hurricane Joaquin. *Geophysical Research Letters*, *52*, e2024GL113531. https://doi.org/10.1029/2024GL113531

Received 3 DEC 2024
Accepted 11 MAY 2025

Author Contributions:

Conceptualization: X. Wu, L. Hoffmann, M. J. Alexander, X. Wang, B. Chen
Data curation: L. Hoffmann, B. Chen
Formal analysis: X. Wu
Funding acquisition: X. Wu, C. J. Wright, N. P. Hindley, M. J. Alexander, X. Wang, B. Chen, Y. Wang
Investigation: X. Wu

1. Introduction

Tropical cyclones (TCs) are hazardous meteorological events that consistently result in loss of life and property. Despite a substantial reduction in track forecast errors over the past decades, predicting abrupt changes in TC intensity, such as rapid intensification (RI), remains challenging (Cangialosi et al., 2020). In addition to being catastrophic weather systems, TCs also serve as sources of excitation for stratospheric gravity waves (GWs) (Hoffmann et al., 2018). Updrafts and thermal forcing due to latent heat release in TCs are the primary mechanisms that generate GWs (Beres et al., 2002). The properties of stratospheric GWs excited by TCs (TC-GWs hereafter) may reflect the thermodynamic and dynamic processes of the TC system, as the mechanisms responsible for exciting these GWs are closely linked to changes in TC intensity. For instance, extremely strong updrafts (often referred to as convective bursts) typically intensify in the eyewall a few hours before TCs reach their peak intensity (Hazelton et al., 2017; H. Wang & Wang, 2014). This process leads to deep latent heating in the upper troposphere, fostering the formation of a warm core (Ohno & Satoh, 2015). Furthermore, the balanced dynamics of TC core structure and flows driven by thermal forcing and deep-layer vertical wind shear contribute to TC intensification (DeHart et al., 2014; Fudeyasu & Wang, 2011; H. Wang & Wang, 2014).

Methodology: X. Wu, L. Hoffmann, C. J. Wright, N. P. Hindley, M. J. Alexander
Project administration: X. Wang
Resources: L. Hoffmann, Y. Wang
Software: X. Wu
Supervision: L. Hoffmann, X. Wang, B. Chen
Visualization: X. Wu
Writing – original draft: X. Wu
Writing – review & editing: X. Wu, L. Hoffmann, C. J. Wright, N. P. Hindley, M. J. Alexander, X. Wang, B. Chen, Y. Wang, M. Li

The connection between the stratospheric GWs intensity and TC intensity was first identified by an idealized model simulation (Nolan & Zhang, 2017), and later verified by multiple long-term satellite observations (Hoffmann et al., 2018; Wright, 2019). Hoffmann et al. (2018) utilized approximately 14 years of observations from Atmospheric Infrared Sounder observations on Aqua to investigate the correlation between TC-GWs and TC intensity. The study indicated that TC-GWs were more intense and active during TC intensification. Statistically, the frequency of TC-GW events during TC intensification was twice as high as during TC weakening. Using 16 years of multiple sources of satellite observations, namely the High-Resolution Dynamics Limb Sounder and Microwave Limb Sounder on Aura, and the Sounding of the Atmosphere using Broadband Emission Radiometry on the Thermosphere, Ionosphere, Mesosphere Energetics and Dynamics satellite, Wright (2019) observed a similar phenomenon: GW amplitudes increased before the peak intensity of TCs, followed by a sudden decrease afterward.

Following the above-mentioned studies based on idealized model simulation and satellite observations, Wu et al. (2022) conducted a high-resolution, realistic model simulation focusing on a specific case, Hurricane Joaquin, which is also the subject of the present study. Wu et al. (2022) also found that intensive GW activity was more frequent during hurricane intensification, particularly for the most intense GWs, which confirmed that the findings by Hoffmann et al. (2018) and Wright (2019) are also valid in a specific case, not only in a statistical sense. These studies supported the hypothesis that stratospheric GWs could be considered as a potential proxy for hurricane intensification.

Observing stratospheric GWs offers an advantageous method for inferring TC intensification, particularly when cloud canopies obscure the TC eye and eyewall from remote sensing instruments using visible and infrared bands. Motivated by the critical need to monitor and accurately predict TC RI, recent research has increasingly focused on using satellite instruments in the infrared and microwave bands for observing TC-GWs, thereby enabling more precise inferences about TC intensity evolution (Miller et al., 2018; Tratt et al., 2018). However, the underlying mechanisms causing the correlation between GW activity and TC intensification are not fully understood. This uncertainty makes the feasibility of monitoring hurricane intensification through observations of stratospheric GWs unclear.

Building upon Wu et al. (2022, hereafter Wu22), this study delves deeper into the mechanism causing the correlation between intense stratospheric GW activity and hurricane intensification. First, we employ a 3-D Stockwell wave analysis method to estimate the properties of the stratospheric GWs, namely the intrinsic frequency and the horizontal and vertical wavelengths. Second, we investigate the properties of GWs and their relationship to the changes in hurricane intensity. The remaining sections are organized as follows: Section 2 describes the model and wave analysis method, Section 3 presents the results, and Section 4 summarizes the results and gives the conclusions.

2. Model and Method

2.1. The High-Resolution WRF Simulation

This study utilized the same Weather Research and Forecasting (WRF) model simulation results of hurricane intensity and stratospheric GWs performed by Wu22. The simulation used a nested configuration with a fixed outer domain (D01) and a vortex-following inner domain (D02). The grid sizes for D01 and D02 were 12 and 4 km, respectively. D01 had a domain size of 210 × 105 grid points, while D02 had a domain size of 201 × 201 grid points. Ninety unevenly spaced sigma levels were set from the surface to 1 hPa, and the topmost 5 km was established as a damping layer. The vertical resolution above 13 km was approximately 500 m, sufficient to resolve GWs with vertical wavelengths exceeding 1 km. The simulation spanned 100 hr, from 00 UTC on 30 September to 04 UTC on 4 October 2015, with outputs recorded at 6-min intervals. The ERA5 reanalysis (Hersbach et al., 2020) provided the initial and boundary conditions of the WRF simulation. The simulation results were compared with observations to ensure that the hurricane intensity and latent heating were accurately simulated. For detailed information on the verification of simulation results, readers are directed to Wu22.

In the following sections, as in Wu22, we focus on analyzing the simulation results from D02, where the simulation results are more accurate regarding hurricane intensity and intensity change and produce more reliable results of the GW features associated with the intensity tendency. Data from the initial 12-hr spin-up period are excluded from the subsequent analyses.

2.2. 3-D Stockwell Wave Analysis Method

The Stockwell transform (Stockwell et al., 1996) is a spectral analysis technique that localizes wave perturbations by applying a scalable Gaussian window to the short-time Fourier transform. This approach enables localized measurements of wavenumber and can be applied to any time series or distance profile. The 3-D Stockwell wave analysis method (Hindley et al., 2016, 2019; Wright et al., 2017) extends the original one-dimensional Stockwell transform to three dimensions, allowing the localization of wavenumbers at every grid point in the 3-D WRF outputs. For the target of wave analysis $h(\boldsymbol{x})$, where $\boldsymbol{x} = (x_1,x_2,x_3)$ is a column vector describing a 3-D coordinate system, the 3-D Stockwell-transform $S(\boldsymbol{\tau},\boldsymbol{f})$ can be written as:

$$S(\boldsymbol{\tau},\boldsymbol{f}) = \frac{1}{(2\pi)^{3/2}} \int_{-\infty}^{\infty} h(\boldsymbol{x}) \left[\prod_{n=1}^{3} \frac{|f_n|}{c_n} e^{\frac{-(x_n-\tau_n)^2 f_n^2}{2c_n^2}} \right] e^{-i2\pi \boldsymbol{f}^{\mathrm{T}} x} d\boldsymbol{x}. \tag{1}$$

Here, $\boldsymbol{\tau} = (\tau_1,\tau_2,\tau_3)$ and $\boldsymbol{f} = (f_1,f_2,f_3)$ are column vectors representing spatial translations and wavenumbers (inverse of wavelength) in the x_1,x_2,x_3 directions. The $\boldsymbol{f}^{\mathrm{T}}$ denotes the transposed $\boldsymbol{f}$. In our case, the target of wave analysis $h(\boldsymbol{x})$ is the vertical velocities from the WRF simulation outputs. We selected the scaling factor $c_n = (c_1,c_2, c_3) = (0.5, 0.5, 0.5)$ which gave a good compromise between spatial and spectral resolution. Additional methodological details regarding the 3-D Stockwell wave analysis are available in Text S1 in Supporting Information S1.

For each WRF output on a 3-D grid (x,y,z), the Stockwell-transform in Equation 1 produces $S(\boldsymbol{\tau},\boldsymbol{f}) \equiv S(\tau_x,\tau_y,\tau_z,f_x,f_y, f_z)$. We then reduced this 6-D object into a 3-D representation by only considering the peak amplitude of the localized (f_x,f_y,f_z) spectrum for each location. We recorded the frequencies at the location of the peak amplitude as the dominant frequencies $F_x(\tau_x,\tau_y,\tau_z)$, $F_y(\tau_x,\tau_y,\tau_z)$, and $F_z(\tau_x,\tau_y,\tau_z)$. In our application, the (τ_x,τ_y,τ_z) domain corresponded to the regular grids (x,y,z) of the WRF outputs, so we got the spatial frequencies $f_x \equiv F_x(x,y,z)$, $f_y \equiv F_y(x,y,z)$, $f_z \equiv F_z(x,y,z)$ which are the inverse of wavelength. Because our WRF grid is cartesian with axes aligned in the zonal, meridional, and vertical directions, f_x, f_y, and f_z are simply the zonal, meridional, and vertical wavenumbers k_0, l_0, and m_0, respectively.

The horizontal wavelength of the GW is calculated as:

$$\lambda_H = \frac{1}{\sqrt{{k_0}^2 + {l_0}^2}}, \tag{2}$$

and the vertical wavelength is:

$$\lambda_Z = \frac{1}{m_0}. \tag{3}$$

The GW intrinsic frequency $\hat{\omega}$ is calculated from the GW dispersion relation (Fritts & Alexander, 2003):

$$\hat{\omega}^2 = \left(\omega - \overline{U}k - \overline{V}l\right)^2 = \frac{N_B^2\left(k^2 + l^2\right) + f^2\left(m^2 + 1/4H^2\right)}{k^2 + l^2 + m^2 + 1/4H^2}, \tag{4}$$

where ω is the ground-based frequency, $\overline{U}$ and $\overline{V}$ are background zonal and meridional wind velocities. $k = 2\pi k_0$, $l = 2\pi l_0$, and $m = 2\pi m_0$. N_B is the Brunt–Väisäla frequency, and H is the scale height (assumed to be 7 km). $f = 2\Omega\sin(\phi)$ is the Coriolis frequency, where Ω is the Earth's rotation rate and ϕ is the latitude.

GW intrinsic phase speed c_{ph} is given by:

$$c_{\mathrm{ph}} = \frac{\hat{\omega}}{k^2 + l^2 + m^2}(k,l,m). \tag{5}$$

2.3. The GROGRAT Gravity Wave Ray-Tracing Model

To investigate the characteristics of GW propagation, we use the GW Regional or Global Ray Tracer (GROGRAT, Eckermann & Marks, 1997; Marks & Eckermann, 1995) to perform ray-tracing of GWs based on the GW dispersion relation. The GROGRAT model used in the current study has been modified particularly for calculations based on WRF model outputs as in previous studies (e.g., S. Wang et al., 2009, 2010; Wei & Zhang, 2015).

The ray tracing equations describe the raypath and refraction along it as follows:

$$\frac{dx_i}{dt} = \frac{\partial \omega}{\partial k_i}, \frac{dk_i}{dt} = \frac{\partial \omega}{\partial x_i}. \tag{6}$$

Via the dispersion relation, these equations are solved based on $\overline{U}$, $\overline{V}$, and N_B background fields. In our study, the background fields were provided by the WRF simulation output and renewed every 6 min. A $(7 \times 7 \times 7)$-boxcar filter was applied to smooth the background fields before using them with GROGRAT to remove the impact of localized gradients. Considering the grid sizes of our simulation, the $(7 \times 7 \times 7)$-boxcar filter proves effective for filtering out fluctuations and deriving the background fields.

3. Results

3.1. Distinct Gravity Wave Properties Associated With Hurricane Intensification Versus Weakening

In this section, we explicitly investigate the properties of stratospheric GWs during the intensification and weakening periods.

First, we calculated the intrinsic frequency, wavelengths, and phase speeds of GWs triggered by the hurricane using the 3-D Stockwell wave analysis method. Figure 1 presents exemplary snapshots of the properties of GWs, including vertical velocities from the WRF simulation as well as the intrinsic frequency, wavelengths, and phase speeds of GWs, captured at 00 UTC on 1 October 2015. These properties are demonstrated at 35 km altitude and along west-east vertical sections crossing the hurricane center. The intrinsic frequency of the stratospheric GWs excited by Hurricane Joaquin is approximately one order of magnitude larger than the Coriolis frequency f and one order of magnitude smaller than the Brunt-Väisälä frequency N_B (Figures 1d–1f), in a frequency range consistent with mid-frequency GWs. The GWs with relatively higher frequency correspond to the inner-core region, including the hurricane's eyewall and the region just outside of it where deep convection occurs actively. These GWs also exhibit shorter horizontal wavelengths (about 20–40 km). The vertical phase speed exceeds twice the horizontal phase speed, resulting in an upward tilt of the vertical propagation angle (greater than 45°).

Next, we analyzed the distribution characteristics of the stratospheric GWs properties separately for the intensification and weakening periods. This was achieved by dividing the values of the intrinsic frequency $\hat{\omega}$, horizontal wavelength λ_H, and vertical wavelength λ_Z into a series of data bins and calculating the occurrence frequency of each property within each bin. The occurrence frequency was normalized with the sum of frequencies equaling 1 for each period. Please refer to Text S2 in Supporting Information S1 for more details.

The analysis was confined to wave properties between 20 and 35 km of altitude. By comparing the background zonal and meridional winds from the WRF simulation to those from the ERA5 reanalysis, we found that the background winds in the stratosphere from the two sources agreed very well below 35 km, but significant differences emerged above approximately 35 km. The differences in the background winds could induce different wave filtering effects, potentially leading to discrepancies in the wave features between the WRF simulation and the ERA5 reanalysis or the real atmosphere. To ensure the reliability of our analysis on the GW properties, we focused exclusively on GWs between 20 and 35 km, thereby avoiding regions where discrepancies existed between the simulation and the ERA5 reanalysis. Please refer to Text S3 in Supporting Information S1 for a detailed comparison of simulated background winds and winds from the ERA5 reanalysis.

As shown in Figure 2, during the hurricane intensification period, the GWs exhibit distinct distributions compared to the weakening period: a greater proportion of GWs have higher intrinsic frequencies ($\hat{\omega} > 2 \times 10^{-3}$ s^{-1}), shorter horizontal wavelengths ($\lambda_H < 40$ km, corresponding to horizontal wavenumbers > 0.025 km^{-1}), and longer vertical wavelengths ($\lambda_Z > 6$ km, corresponding to vertical wavenumbers < 0.167 km^{-1}). Particularly, GWs with

10.1029/2024GL113531

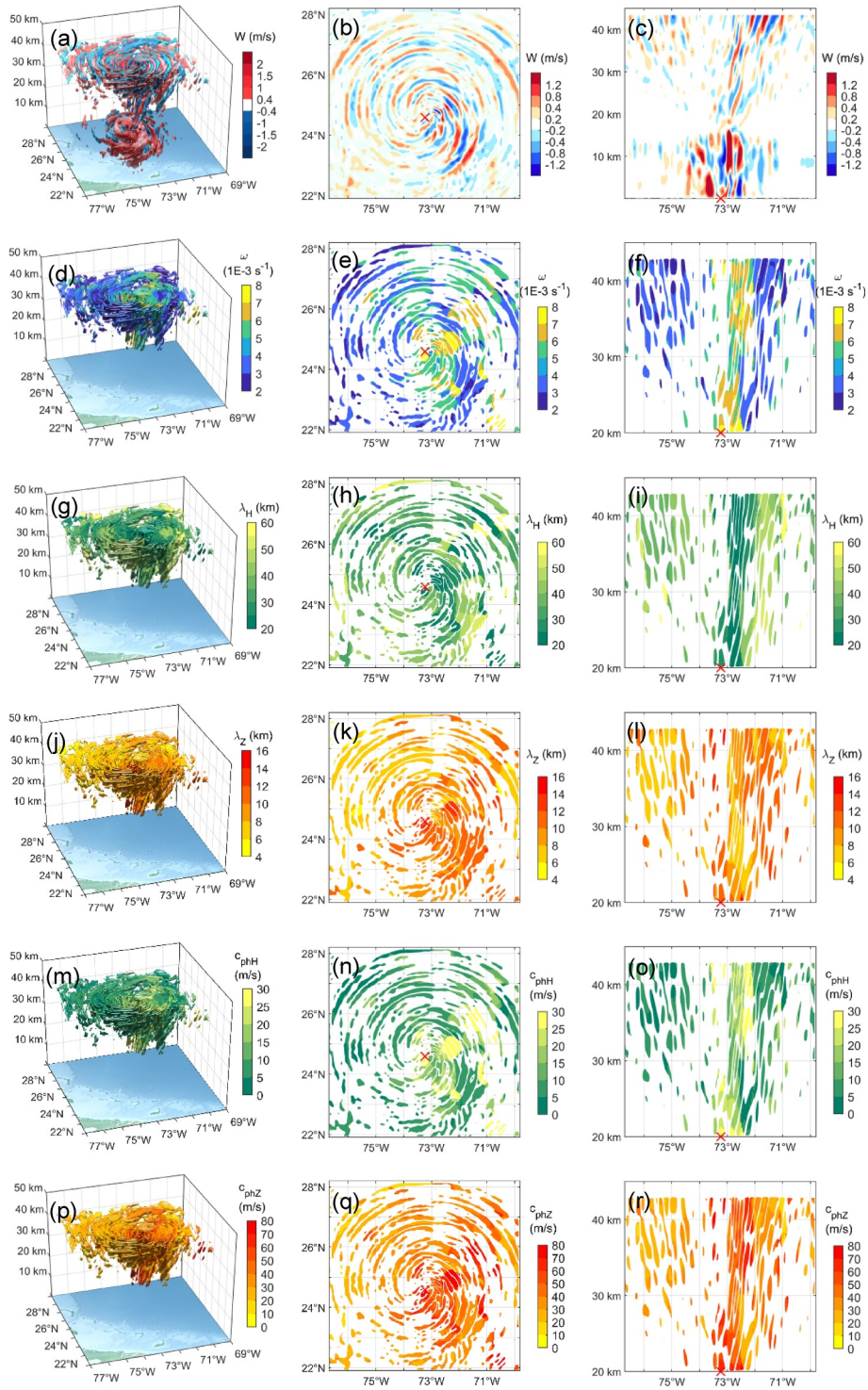

Figure 1. Properties of stratospheric gravity waves excited by Hurricane Joaquin (2015): (a–c) Weather Research and Forecasting simulated vertical velocities w, (d–f) 3-D Stockwell analysis estimated intrinsic frequency $\hat{\omega}$, (g–i) horizontal wavelength λ_H, (j–l) vertical wavelength λ_Z, (m–o) intrinsic horizontal phase speed c_{phH}, and (p–r) intrinsic vertical phase speed c_{phZ}. Plots in the left column show the 3-D features, plots in the middle column depict the features at 35 km, and those in the right column present a west-east vertical cross-section. Only waves of amplitudes larger than 0.2 m/s and their properties are shown. The red crosses in the middle and right columns indicate the hurricane center.

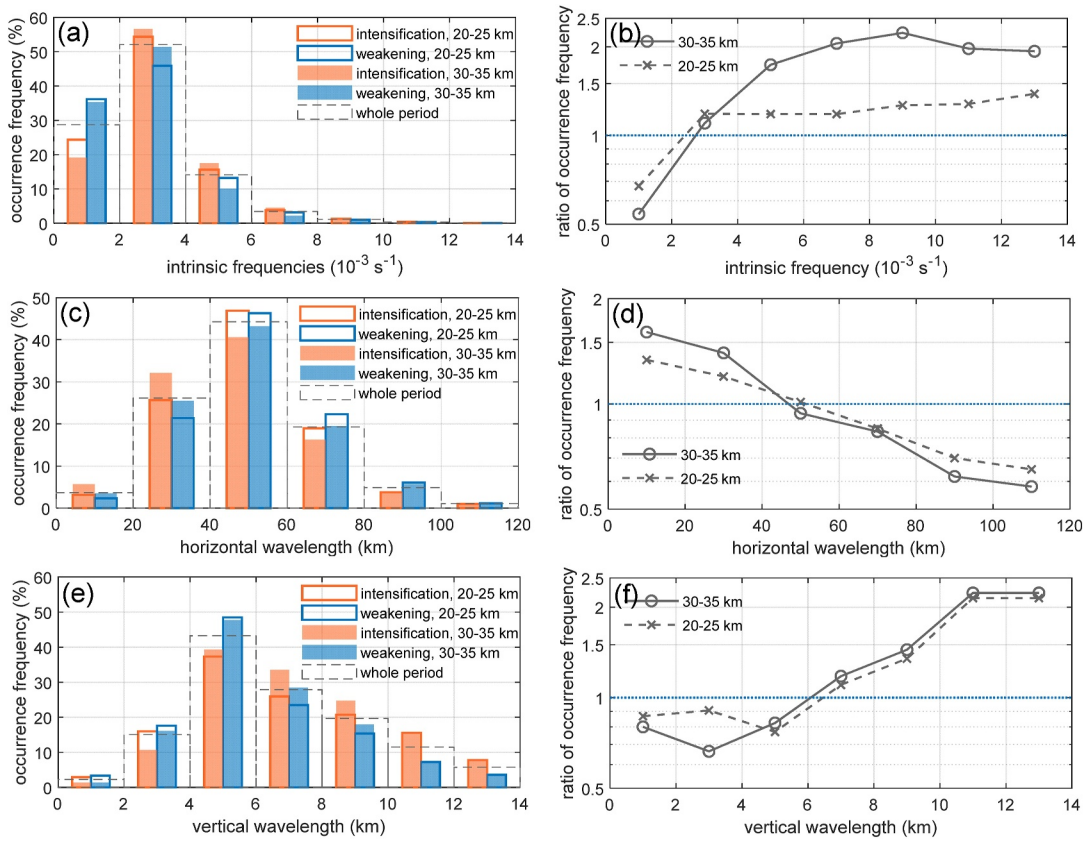

Figure 2. The occurrence frequency of stratospheric gravity wave properties and the ratio between the intensification and weakening periods. (a, b) Intrinsic frequency $\hat{\omega}$, (c, d) horizontal wavelengths λ_H, and (e, f) vertical wavelengths λ_Z, separately during hurricane intensification and weakening at the altitude ranges of 20–25 and 30–35 km. The occurrence frequency for the whole simulation period at 20–35 km is superimposed for comparison (gray dashed line).

$\hat{\omega} > 6 \times 10^{-3}$ s^{-1}, $\lambda_H < 20$ km, and $\lambda_Z > 10$ km are approximately twice as likely to occur during the intensification period. This result aligns with a previous simulation study on Typhoon Saomai (2006), which noted a shift in the horizontal wavelength spectral peak at 20 km altitude. During the intensification period, the spectral peak was observed at shorter wavelengths, while during the weakening period, it shifted to around 60 km (Kim & Chun, 2010). Sensitive studies have been conducted to confirm that the distinct wave properties, that is, higher $\hat{\omega}$, shorter λ_H, and longer λ_Z are robust across a reasonable range of scaling factors in Equation 1 (see details in Figure S1 in Supporting Information S1). As GWs propagate from the lower stratosphere (20–25 km) to the middle stratosphere (30–35 km), the contrasts between the intensification and weakening scenarios in the distribution of the above three properties become more prominent. This is probably because higher-frequency GWs are less likely to be dissipated or reflected at critical levels, and shorter-wavelength GWs can carry more momentum flux, thereby enhancing the wave's vertical propagation capabilities.

Previous studies have demonstrated that the dominant horizontal and vertical wavelengths of the GWs excited by convection are closely related to the width and the depth of the thermal force in the convection (e.g., Alexander et al., 1995; Pandya & Alexander, 1999). By analyzing the relationship between the GW wavelengths and the scale of latent heating in the hurricane's inner core (see details in Text S4 in Supporting Information S1), we confirm that during the intensification period of Hurricane Joaquin, the tropospheric heating is relatively narrower and deeper than during the weakening period, leading to shorter horizontal wavelengths and longer vertical wavelengths.

Wu22 discovered that the occurrence frequency of stratospheric GWs of large intensity was larger during the intensification period compared to the weakening period. Following Wu22, we defined the GW intensity as the mean vertical velocity variance σ^2 between 20 and 35 km, and analyzed the relationship between the GW intensity

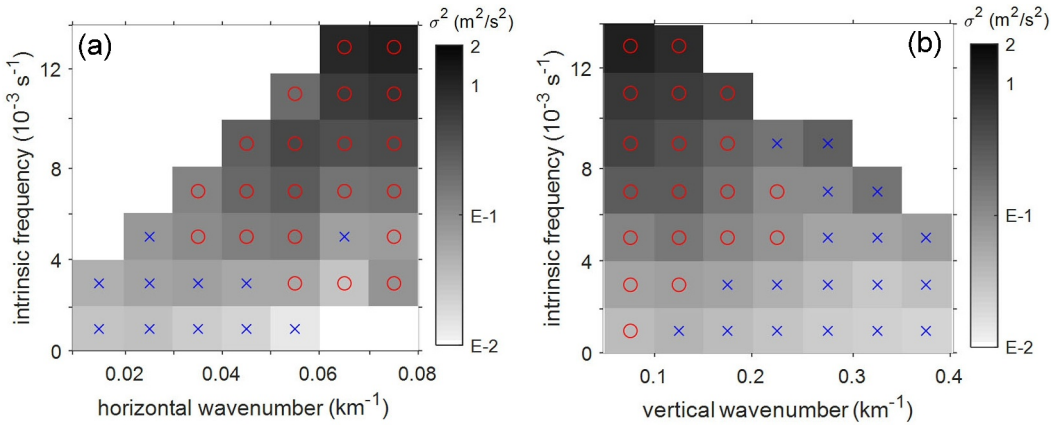

Figure 3. Gravity wave intensity represented by the mean vertical velocity variances σ^2 in the domains of (a) horizontal wavenumber and intrinsic frequency and (b) vertical wavenumber and intrinsic frequency. Bins marked with red circles show higher proportions during hurricane intensification, while those marked with blue crosses exhibit higher proportions during hurricane weakening.

and the GW frequencies and wavelengths. Through GW intensity spectrum analysis, we confirm that high-intensity GWs are predominantly composed of those GWs with higher intrinsic frequencies, smaller horizontal wavenumbers, and larger vertical wavenumbers (Figure 3). These GWs are predominantly excited during hurricane intensification, which explains the finding of Wu22.

3.2. The Propagation Characteristics of Gravity Waves During Hurricane Intensification and Weakening

Wu22 found that during the intensification period, there was a relatively clear sequence in the changes of GW intensity and hurricane intensity: changes in stratospheric GW intensity usually preceded changes in hurricane intensity, which indicated increasingly intense stratospheric GW activity could serve as a potential indicator for hurricane intensification. In contrast, during the weakening period, the above sequence was unclear. This difference found in Wu22 is likely attributable to the propagation characteristics of GWs from the source to the stratosphere. Therefore, we employ the GROGRAT ray-tracing model to study the propagation characteristics of GWs separately during the intensification and weakening periods.

Using the GROGRAT ray-tracing model, we traced GWs with amplitudes in vertical velocities (w) greater than 0.2 m/s at 32 km altitude back to their source. We calculated their propagation time and the distance they propagate away from their initial location in the horizontal dimension. We did not differentiate between specific horizontal directions when calculating the horizontal distance. The waves whose inferred raypath terminated by the GROGRAT model at altitudes higher than 18 km were excluded. These waves either approached a critical level from above or the wave amplitude vanished. Meanwhile, we examined the derived GW phase speeds and frequencies along the inferred ray paths to ensure the sources of the GWs are convection within the hurricane.

Figure 4 shows the propagation time and the horizontal propagation distance of the GWs we traced from 32 km downward to 18 km. The color shading in Figure 4a shows that during the intensification period, 100% of the GWs can be traced downward from 32 to 28 km in less than 5 min. Most of the GWs can be traced downward from 32 to 26 km in less than 5 min, but a fraction of the GWs take up to 10 min to propagate through the same vertical distance. Generally, GWs during the intensification period have longer vertical wavelengths and higher intrinsic frequencies. Consequently, they take a relatively shorter time (less than 20 min) to propagate from 18 km upward to 32 km, with some very fast GWs taking less than 5 min. These GWs do not travel far horizontally from their source, covering distances up to 40 km, as seen in Figure 4c. In contrast, Figure 4b shows that there is a larger spread in propagation time during the weakening period. GWs take up to 1 hr to propagate from 18 km upward to 32 km, and the waves travel up to 80 km horizontally during that time, as illustrated in Figure 4d. As examples, the propagation of two pairs of GWs with the same initial vertical wavelengths but distinct intrinsic frequencies and horizontal wavelengths is superimposed. The waves with lower intrinsic frequency and longer horizontal wavelength propagate upward more slowly and can travel further from the source while ascending through the same vertical range.

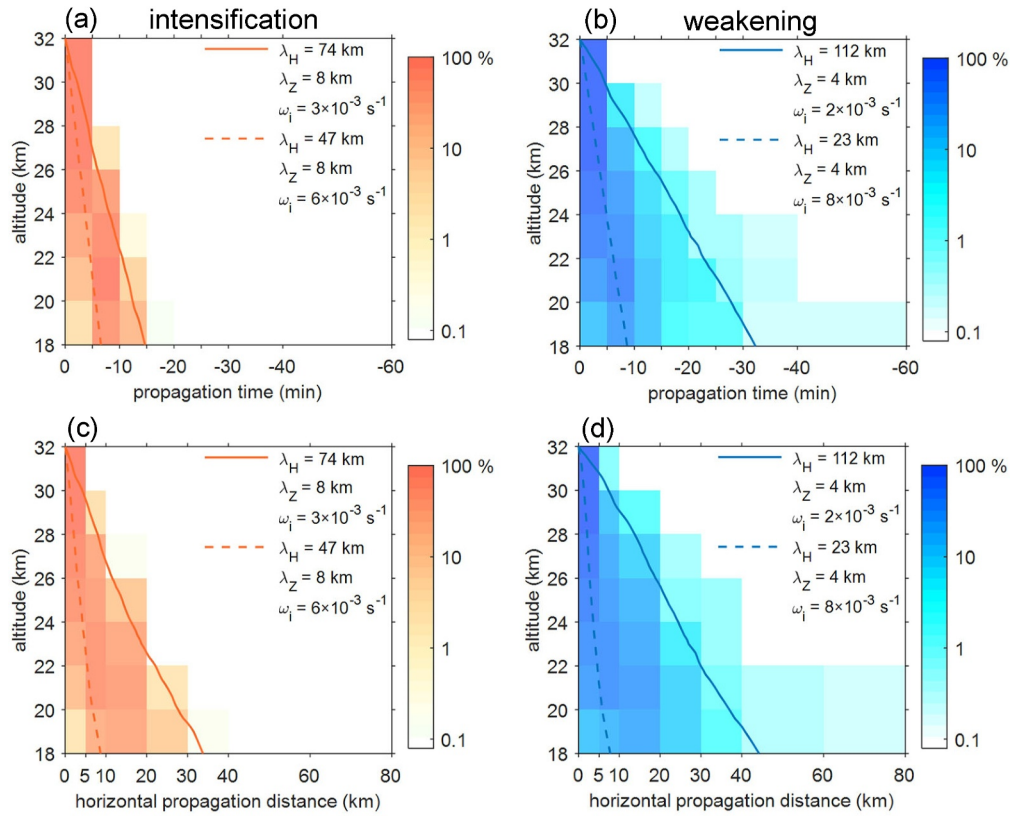

Figure 4. (a, b) The occurrence frequency of the propagation time from 32 km downward to 18 km and the (c, d) horizontal propagation distance during this propagation time for both the intensification and weakening periods. On each panel, the propagation time or horizontal propagation distance from two gravity waves with the same initial vertical wavelengths but distinct initial horizontal wavelengths and intrinsic frequencies is superimposed. The solid line indicates the wave with a longer horizontal wavelength, and the dashed line indicates the wave with a shorter horizontal wavelength.

Previous research has shown that strong updrafts appear 0–3 hr before TC intensification (e.g., Hazelton et al., 2017). These updrafts produce deep latent heating in the upper troposphere, consequently triggering GWs. These triggered GWs require additional time to propagate from the source to the middle stratosphere. Therefore, fast vertically propagating GWs triggered during hurricane intensification are more likely to be observed in the stratosphere before the hurricane reaches its peak intensity, making them a potential indicator for hurricane intensification. And the stratospheric GWs that may indicate hurricane intensification are expected to appear above the region of deep latent heating, as their horizontal propagation is limited during their upward propagation.

4. Conclusions

In the previous study of Wu22, a realistic WRF model simulation of stratospheric GWs excited by Hurricane Joaquin was conducted. Wu22 identified a robust correlation between intensive stratospheric GWs and hurricane intensification. It is found that the occurrence frequency of intense stratospheric GWs was larger during hurricane intensification than weakening, and changes in GW intensity preceded the changes in hurricane intensity during the intensification period, making intense GW activity a potential proxy for hurricane intensification. This present study further investigated the mechanism behind the findings of Wu22 by analyzing the distinct GW properties and wave propagation characteristics during the intensification and weakening periods of the hurricane. First, the 3-D Stockwell wave analysis method was used to estimate the 3-D properties of the stratospheric GWs generated by the hurricane. We identified distinct properties of the GWs during the intensification of Hurricane Joaquin. These properties included relatively higher intrinsic frequency ($>2 \times 10^{-3}$ s^{-1}), shorter horizontal wavelengths (<40 km), and longer vertical wavelengths (>6 km). Additionally, the upper range of the GW intensity spectrum was dominated by GWs with these properties. This explained why intense GWs occurred more frequently during hurricane intensification. Furthermore, by analyzing the GW propagation characteristics using the GROGRAT

ray-tracing model, we found that the GWs excited during hurricane intensification exhibited rapid vertical speed, and the time required for them to propagate from 18 km upward to 32 km in the stratosphere was less than 20 min. This duration may be shorter than the time it takes for the hurricane to reach its peak intensity, suggesting that these intense GWs could appear in the stratosphere during hurricane intensification. Therefore, the intense GW activities could be considered a proxy for hurricane intensification. Conversely, during the weakening period, the vertical propagation of GWs was relatively slower, making the sequence of the changes in hurricane intensity and GW intensity less clear.

Hurricane Joaquin was one of the cases with a relatively high correlation coefficient between GW intensity and hurricane intensity change (Hoffmann et al., 2018; Wu et al., 2022), enabling a detailed examination of the wave properties and propagation under favorable atmospheric background conditions. However, in a broader context, the relationship between stratospheric GW and TC intensity changes involves additional considerations, including the modulation of wave properties by background winds and the inherently complex nature of TC intensity changes. This study serves as an initial step toward understanding the mechanisms that link stratospheric GW activity to TC intensity changes. Expanding this understanding to encompass a broader range of cases across diverse meteorological conditions will be an important direction for future research.

Data Availability Statement

The ERA5 reanalysis data (Hersbach et al., 2023) were retrieved from the ECMWF Meteorological Archival and Retrieval System (10.24381/cds.bd0915c6; last accessed: 27 October 2024). The 3-D Stockwell wave analysis method codes (Hindley, 2021) are archived and freely available at https://doi.org/10.5281/zenodo.4721882.

Acknowledgments

X. Wu is supported by the National Natural Science Foundation of China (NSFC) Grant 42475068 and the Strategy Priority Research Program of the Chinese Academy of Sciences Grant XDB0760101. CJW is supported by the Royal Society University Research Fellowship URF\R \221023, and NERC Grants NE/S00985X/1 and NE/V01837X/1. NPH is supported by the NERC Independent Research Fellowship NE/X017842/1. MJA was supported by NASA Weather and Atmospheric Dynamics Program Grant 80NSSC23K1311. BC is supported by the NSFC Grants 42175046 and 42065009, and the Natural Science Foundation of Yunnan Province Grant 201901BB050045. X. Wang is supported by the Strategy Priority Research Program of the Chinese Academy of Sciences Grant XDB0760101. YNW is supported by the second Tibetan Plateau Scientific Expedition and Research Program Grant 2019QZKK0604. The computing time and storage were provided by the Juelich Supercomputing Centre. We gratefully acknowledge Dr. Shuguang Wang from Nanjing University and Dr. Junhong Wei from Sun Yat-sen University for their technical support in the ray tracing model.

References

Alexander, M. J., Holton, J. R., & Durran, D. R. (1995). The gravity wave response above deep convection in a squall line simulation. *Journal of the Atmospheric Sciences*, *52*(12), 2212–2226. https://doi.org/10.1175/1520-0469(1995)052<2212:Tgwrad>2.0.Co;2

Beres, J. H., Alexander, M. J., & Holton, J. R. (2002). Effects of tropospheric wind shear on the spectrum of convectively generated gravity waves. *Journal of the Atmospheric Sciences*, *59*(11), 1805–1824. https://doi.org/10.1175/1520-0469(2002)059<1805:Eotwso>2.0.Co;2

Cangialosi, J. P., Blake, E., DeMaria, M., Penny, A., Latto, A., Rappaport, E., & Tallapragada, V. (2020). Recent progress in tropical cyclone intensity forecasting at the National Hurricane Center. *Weather and Forecasting*, *35*(5), 1913–1922. https://doi.org/10.1175/WAF-D-20-0059.1

DeHart, J. C., Houze, R. A., & Rogers, R. F. (2014). Quadrant distribution of tropical cyclone inner-core kinematics in relation to environmental shear. *Journal of the Atmospheric Sciences*, *71*(7), 2713–2732. https://doi.org/10.1175/JAS-D-13-0298.1

Eckermann, S. D., & Marks, C. J. (1997). GROGRAT: A new model of the global propagation and dissipation of atmospheric gravity waves. *Advances in Space Research*, *20*(6), 1253–1256. https://doi.org/10.1016/S0273-1177(97)00780-1

Fritts, D. C., & Alexander, M. J. (2003). Gravity wave dynamics and effects in the middle atmosphere. *Reviews of Geophysics*, *41*(1), 1003. https://doi.org/10.1029/2001RG000106

Fudeyasu, H., & Wang, Y. (2011). Balanced contribution to the intensification of a tropical cyclone simulated in TCM4: Outer-core spinup process. *Journal of the Atmospheric Sciences*, *68*(3), 430–449. https://doi.org/10.1175/2010jas3523.1

Hazelton, A. T., Hart, R. E., & Rogers, R. F. (2017). Analyzing simulated convective bursts in two Atlantic hurricanes. Part II: Intensity change due to bursts. *Monthly Weather Review*, *145*(8), 3095–3117. https://doi.org/10.1175/mwr-d-16-0268.1

Hersbach, H., Bell, B., Berrisford, P., Biavati, G., Horányi, A., Muñoz Sabater, J., et al. (2023). ERA5 hourly data on pressure levels from 1940 to present [Dataset]. *Copernicus Climate Change Service (C3S) Climate Data Store (CDS)*. https://doi.org/10.24381/cds.bd0915c6

Hersbach, H., Bell, B., Berrisford, P., Hirahara, S., Horányi, A., Muñoz-Sabater, J., et al. (2020). The ERA5 global reanalysis. *Quarterly Journal of the Royal Meteorological Society*, *146*(730), 1999–2049. https://doi.org/10.1002/qj.3803

Hindley, N. P. (2021). Three-dimensional Stockwell transform: April 26, 2021 release (version 1.0.0) [Software]. *Zenodo*. https://doi.org/10.5281/zenodo.4721882

Hindley, N. P., Smith, N. D., Wright, C. J., Rees, D. A. S., & Mitchell, N. J. (2016). A two-dimensional Stockwell transform for gravity wave analysis of AIRS measurements. *Atmospheric Measurement Techniques*, *9*(6), 2545–2565. https://doi.org/10.5194/amt-9-2545-2016

Hindley, N. P., Wright, C. J., Smith, N. D., Hoffmann, L., Holt, L. A., Alexander, M. J., et al. (2019). Gravity waves in the winter stratosphere over the southern ocean: High-resolution satellite observations and 3-D spectral analysis. *Atmospheric Chemistry and Physics*, *19*(24), 15377–15414. https://doi.org/10.5194/acp-19-15377-2019

Hoffmann, L., Wu, X., & Alexander, M. J. (2018). Satellite observations of stratospheric gravity waves associated with the intensification of tropical cyclones. *Geophysical Research Letters*, *45*(45), 1692–1700. https://doi.org/10.1002/2017GL076123

Kim, S.-Y., & Chun, H.-Y. (2010). Stratospheric gravity waves generated by typhoon Saomai (2006): Numerical modeling in a moving frame following the typhoon. *Journal of the Atmospheric Sciences*, *67*(11), 3617–3636. https://doi.org/10.1175/2010JAS3374.1

Marks, C. J., & Eckermann, S. D. (1995). A 3-dimensional nonhydrostatic ray-tracing model for gravity waves formulation and preliminary results for the middle atmosphere. *Journal of the Atmospheric Sciences*, *52*(11), 1959–1984. https://doi.org/10.1175/1520-0469(1995)052<1959:Atdnrt>2.0.Co;2

Miller, S. D., Straka, W. C., Yue, J., Seaman, C. J., Xu, S., Elvidge, C. D., et al. (2018). The dark side of hurricane Matthew: Unique perspectives from the VIIRS day/night band. *Bulletin of the American Meteorological Society*, *99*(12), 2561–2574. https://doi.org/10.1175/bams-d-17-0097.1

Nolan, D. S., & Zhang, J. A. (2017). Spiral gravity waves radiating from tropical cyclones. *Geophysical Research Letters*, *44*(8), 3924–3931. https://doi.org/10.1002/2017GL073572

Ohno, T., & Satoh, M. (2015). On the warm core of a tropical cyclone formed near the tropopause. *Journal of the Atmospheric Sciences*, *72*(2), 551–571. https://doi.org/10.1175/jas-d-14-0078.1

Pandya, R. E., & Alexander, M. J. (1999). Linear stratospheric gravity waves above convective thermal forcing. *Journal of the Atmospheric Sciences*, *56*(14), 2434–2446. https://doi.org/10.1175/1520-0469(1999)056<2434:Lsgwac>2.0.Co;2

Stockwell, R. G., Mansinha, L., & Lowe, R. P. (1996). Localization of the complex spectrum: The S transform. *IEEE Transactions on Signal Processing*, *44*(4), 998–1001. https://doi.org/10.1109/78.492555

Tratt, D. M., Hackwell, J. A., Valant-Spaight, B. L., Walterscheid, R. L., Gelinas, L. J., Hecht, J. H., et al. (2018). GHOST: A satellite mission concept for persistent monitoring of stratospheric gravity waves induced by severe storms. *Bulletin of the American Meteorological Society*, *99*(9), 1813–1828. https://doi.org/10.1175/bams-d-17-0064.1

Wang, H., & Wang, Y. (2014). A numerical study of typhoon Megi (2010). Part I: Rapid intensification. *Monthly Weather Review*, *142*(1), 29–48. https://doi.org/10.1175/mwr-d-13-00070.1

Wang, S., Zhang, F., & Epifanio, C. C. (2010). Forced gravity wave response near the jet exit region in a linear model. *Quarterly Journal of the Royal Meteorological Society*, *136*(652), 1773–1787. https://doi.org/10.1002/qj.676

Wang, S., Zhang, F., & Snyder, C. (2009). Generation and propagation of inertia-gravity waves from vortex dipoles and jets. *Journal of the Atmospheric Sciences*, *66*(5), 1294–1314. https://doi.org/10.1175/2008jas2830.1

Wei, J., & Zhang, F. (2015). Tracking gravity waves in moist baroclinic jet-front systems. *Journal of Advances in Modeling Earth Systems*, *7*(1), 67–91. https://doi.org/10.1002/2014ms000395

Wright, C. J. (2019). Quantifying the global impact of tropical cyclone-associated gravity waves using HIRDLS, MLS, SABER and IBTrACS data. *Quarterly Journal of the Royal Meteorological Society*, *145*(724), 3013–3039. https://doi.org/10.1002/qj.3602

Wright, C. J., Hindley, N. P., Hoffmann, L., Alexander, M. J., & Mitchell, N. J. (2017). Exploring gravity wave characteristics in 3-D using a novel S-transform technique: AIRS/Aqua measurements over the Southern Andes and Drake Passage. *Atmospheric Chemistry and Physics*, *17*(13), 8553–8575. https://doi.org/10.5194/acp-17-8553-2017

Wu, X., Hoffmann, L., Wright, C. J., Hindley, N. P., Kalisch, S., Alexander, M. J., & Wang, Y. (2022). Stratospheric gravity waves as a proxy for hurricane intensification: A case study of weather research and forecast simulation for hurricane Joaquin. *Geophysical Research Letters*, *49*(1), e2021GL097010. https://doi.org/10.1029/2021GL097010